Key Points:
- Both increases and decreases in neutral temperature are seen at low and middle latitudes in the mesosphere and lower thermosphere (MLT) region during storms
- There is a time delay in storm time MLT temperature changes; the onset of the changes occurs first at night and at higher latitudes
- The storm time temperature changes at middle and low latitudes in the MLT region are mostly caused by adiabatic heating/cooling associated with vertical wind variations

Correspondence to:
J. Lu,
jylu@nuist.edu.cn

On the Responses of Mesosphere and Lower Thermosphere Temperatures to Geomagnetic Storms at Low and Middle Latitudes

Jingyuan Li[1,2] (iD), Wenbin Wang[2] (iD), Jianyong Lu[1] (iD), Tao Yuan[3] (iD), Jia Yue[4,5] (iD), Xiao Liu[6,7] (iD), Kedeng Zhang[8] (iD), Alan G. Burns[2] (iD), Yongliang Zhang[9] (iD), and Zheng Li[1,2] (iD)

[1]Institute of Space Weather, College of Math and Statistics, Nanjing University of Information Science and Technology, Nanjing, China, [2]High Altitude Observatory, National Center for Atmospheric Research, Boulder, CO, USA, [3]Center for Atmospheric and Space Sciences, Utah State University, Logan, UT, USA, [4]Atmospheric and Planetary Sciences, Hampton University, Hampton, VA, USA, [5]ESSIC, University of Maryland, College Park, MD, USA, [6]Henan Engineering Laboratory for Big Data Statistical Analysis and Optimal Control, School of Mathematics and Information Science, Henan Normal University, Xinxiang, China, [7]State Key Laboratory of Space Weather, National Space Science Center, Chinese Academy of Sciences, Beijing, China, [8]Department of Space Physics, School of Electronic Information, Wuhan University, Wuhan, China, [9]Applied Physics Laboratory, Johns Hopkins University, Laurel, MD, USA

Abstract Observations from lidars and satellites have shown that large neutral temperature increases and decreases occur in the middle and low latitudes of the mesosphere and lower thermosphere region during geomagnetic storms. Here we undertake first-principles simulations of mesosphere and lower thermosphere temperature responses to storms using the Thermosphere Ionosphere Mesosphere Electrodynamics General Circulation Model to elucidate the nature and causes of these changes. Temperature variations were not uniform; instead, nighttime temperatures changed earlier than daytime temperatures, and temperatures changed earlier at high latitudes than at low ones. Furthermore, temperatures increased in some places/times and decreased in others. As the simulation behaves similar to observations, it provides an opportunity to understand physical processes that drive the observed changes. Our analysis has shown that they were produced mainly by adiabatic heating/cooling that was associated with vertical winds resulting from general circulation changes, with additional contributions from vertical heat advection.

Plain Language Summary Both ground- and space-based observations have showed that storm time temperature have strong variations in the mesosphere and lower thermosphere (MLT) region. However, the possible physical mechanisms causing these storm time thermal responses have not been fully understood. Therefore, in this paper, we use the Thermosphere Ionosphere Mesosphere Electrodynamics General Circulation Model to investigate the possible mechanisms for the observed storm time temperature changes in the MLT region. As the simulation behaves similar to observations, it provides an opportunity to understand physical processes that drive the observed changes. By analyzing Thermosphere Ionosphere Mesosphere Electrodynamics General Circulation Model results, we found storm time adiabatic heating/cooling and vertical heat advection, both associated with changes in vertical winds, are the MLT-dominant heating processes in the MLT region at middle latitudes. Horizontal heat advection and radiative cooling also contribute to temperature changes, but they occur later than the other major heating terms. At middle and low latitudes, MLT changes are first seen in the vertical winds, followed by temperature changes; horizontal winds change later. The changes of vertical winds in the MLT region are associated with those occurring at higher altitudes. There is no direct contribution of auroral Joule heating and particle heating to the storm time MLT temperature changes at middle latitudes.

1. Introduction

During geomagnetic storms, the enhanced auroral precipitation and electric fields at high latitudes result in strong Joule heating and ion drag, which, in turn, change neutral temperatures (T_n), composition, winds, and ionospheric electron densities in the polar region. These changes are then transmitted globally to other regions and altitudes through dynamic and chemical processes (Banks, 1977; Rees et al., 1983; Roble et al., 1987). Storm effects on the upper thermosphere have been an area of active research and great understanding of the physical processes driving these effects have been obtained (e.g., Fejer et al., 2017;

Förster & Jakowski, 2000; Fuller-Rowell et al., 1994; Liu et al., 2016; Mendillo et al., 1972). However, assessing storm effects on the mesosphere and lower thermosphere (MLT) region has been a challenge. The lack of observations, combined with the complex physical and chemical processes that occur in this region, makes it difficult to determine the nature and causes of possible storm time MLT changes.

Temperature changes have been detected globally during strong storms in the MLT region (e.g., Biondi & Meriwether, 1985; Fagundes et al., 1996; Von Savigny et al., 2007). Pancheva et al. (2007) showed a greater than 25-K drop in temperature around 90 km. They suggested that the temperature changes might be associated with a reduction of ozone, caused by energetic particle precipitation. Nesse Tyssøy et al. (2008, 2010) showed that T_n was increased above 90 km during a relatively strong storm event. They suggested that T_n increase above 100 km was associated with auroral heating, which includes both precipitation particle heating and Joule heating, whereas temperature changes below 100 km were not directly related to such auroral heating. Fang et al. (2008) and Xu et al. (2013) further demonstrated that auroral heating effects on temperature can penetrate down to the altitudes of ~105 km at high latitudes during storms. Researchers also proposed that the temperature and dynamics within the polar cap region can be impacted by energetic particle precipitation and Joule heating, which then lead to composition changes affecting atmospheric heating and cooling rates, general circulation, and wave propagation and breaking (Sinnhuber et al., 2012). Recently, Yuan et al. (2015), using Na lidar data, found that in the four geomagnetic storms of 17 April 2002, 6 November 2004, 8 May 2005, and 1 October 2012, there were large changes in midlatitude MLT temperatures. A maximum nightly mean temperature increase of 44 K at 105 km was observed from the Na lidar (41°N, 105°W) between 95 and 106 km during the 18 April 2002 storm. They also found that temperature changes were correlated with the storm time depletion of thermospheric column density of O/N$_2$. Liu et al. (2018) studied the effects of the 2013 St. Patrick's Day storm on MLT temperature using satellite data. The storm time warming was larger than 15 K above 100 km and ~10 K below 100 km at middle latitudes. They proposed that temperature changes might be related to the storm time variation in global circulation caused by energy and momentum inputs in the auroral region.

Therefore, both ground- and space-based observations, although very limited, have shown that T_n can have strong variations in the MLT region during storms. However, most of the previous studies are focused on the direct effects of energetic particle precipitation through chemical processes. The possible physical mechanisms that have been suggested for storm time T_n change, including Joule heating, energetic particle precipitation, and general circulation, have not been fully and self-consistently examined in the context of the global, coupled, mesosphere, thermosphere, and ionosphere system. Furthermore, the interplay between various physical processes in the MLT region during storms is not fully understood, leaving the cause of storm time global thermal response in the region unclear.

In this paper, we use the Thermosphere Ionosphere Mesosphere Electrodynamics General Circulation Model (TIMEGCM; Roble & Ridley, 1994) to investigate the possible mechanisms for the storm time temperature changes in the MLT region during the storm event of 17 April 2002. By diagnostically analyzing TIMEGCM outputs, we have obtained new insights into the processes that cause the simulated MLT temperature changes.

2. Model Simulations

The TIMEGCM is a three-dimensional global model that self-consistently simulates temperature, circulation, dynamics, photoionization, electrodynamics, chemistry, and composition of Earth's middle and upper atmosphere. The model horizontal resolution is 2.5° × 2.5° in geographic latitude and longitude. The vertical coordinate is pressure level with a resolution of one-fourth scale height. For the TIMEGCM runs in this paper, the high-latitude ion convection pattern is specified by the Heelis model (Heelis et al., 1982) and is driven by the 3-hr Kp index.

A diagnostic analysis of the TIMEGCM outputs has been carried out to investigate the possible physical processes that cause temperature changes in the MLT region between the altitudes of 94–110 km during the storm event of 17 April 2002 (Figure 1). Two TIMEGCM runs were performed: One was driven with the true geophysical conditions, and the other by a constant Kp value of 3.0 for geomagnetically nondisturbed conditions. The Kp value of 3.0 was chosen since it was the value between 00:00 and 06:00 UT for the
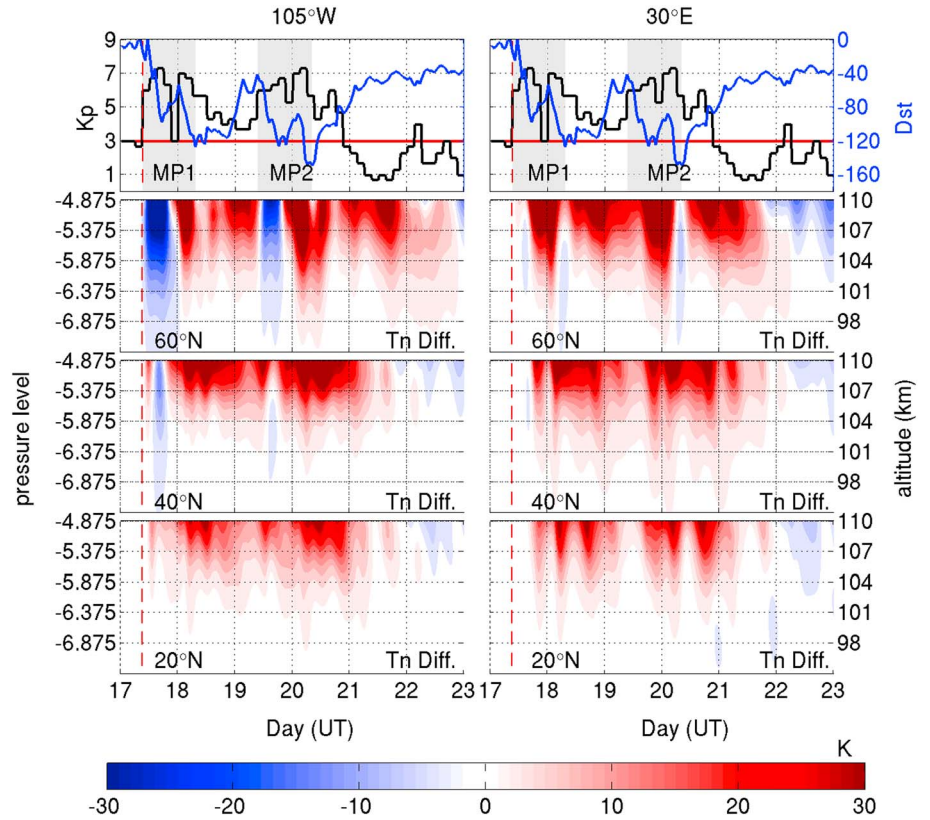
Figure 1. (top row) *Kp* (black line) and *Dst* (blue line) between 17 and 23 April 2002: The black solid line shows the real *Kp* during the storm, and the red line is a constant *Kp* value of 3.0 for nondisturbed conditions. The second to bottom rows are the T_n differences at 60°N, 40°N, and 20°N from 94 to 110 km between TIMEGCM simulations driven by the real *Kp* and by a constant *Kp* value of 3.0. The left column is for the longitude of 105°W where the storm began at 02:00 LT. The right column is for the longitude of 30°E and the onset of the storm was at 11:00 LT. The red dashed lines indicate the beginning of the geomagnetic storm.

conditions on 17 April 2002, just before the storm (top panels in Figure 1). The two model runs began with exactly the same model history at 00:00 UT on 17 April. Thus, the difference between the two-model results represents the impacts of the storm in the MLT region.

T_n is calculated by solving the thermodynamic equation:

$$\frac{\partial T_n}{\partial t} = \frac{ge^z}{p_0 C_p} \frac{\partial}{\partial Z} \left\{ \frac{K_T}{H} \frac{\partial T_n}{\partial Z} + K_E H^2 C_p \rho \left[\frac{g}{C_p} + \frac{1}{H} \frac{\partial T}{\partial Z} \right] \right\} - \overrightarrow{v}_n \cdot \nabla T_n - W \left(\frac{\partial T_n}{\partial Z} + \frac{R^* T_n}{C_p \, \bar{m}} \right) + \frac{Q - L}{C_p}, \qquad (1)$$

where t is the time and g is the gravitational acceleration. C_p is the specific heat per unit mass for constant pressure, K_T is the molecular thermal conductivity, H is the pressure scale height, K_E is the eddy diffusion coefficient, ρ is the atmospheric mass density, $\overrightarrow{v}_n$ is the horizontal velocity, W is the vertical wind velocity, R^* is the universal gas constant, and $\bar{m}$ is the mean molecular mass. The terms on the right-hand side are the heat transfer by vertical molecular heat conduction ($\frac{ge^z}{p_0 C_p} \frac{\partial}{\partial Z} \left\{ \frac{K_T}{H} \frac{\partial T_n}{\partial Z} \right\}$), eddy diffusion ($\frac{ge^z}{p_0 C_p} \frac{\partial}{\partial Z} \left\{ K_E H^2 C_p \rho \left[\frac{g}{C_p} + \frac{1}{H} \frac{\partial T}{\partial Z} \right] \right\}$), and horizontal advection ($v_n \cdot \nabla T_n$), adiabatic heating/cooling ($W \frac{R^* T_n}{C_p \, \bar{m}}$), vertical heat advection ($W \frac{\partial T_n}{\partial Z}$), and other heating and cooling processes (Q and L), including solar, chemical and Joule heating, and NO and CO_2 infrared radiative cooling. By comparing each term from those two runs, we obtain their relative importance for the simulated storm time temperature changes and therefore, understand the physical mechanisms driving these changes.

3. Results

Yuan et al. (2015) showed the storm effects on MLT temperatures during four storm events of 17 April 2002, 6 November 2004, 8 May 2005, and 1 October 2012 using the nocturnal Na lidar data at two close midlatitude stations. They observed significant nighttime temperature enhancements in the lower thermosphere during those storms, but the magnitude of the maximum temperature increase was different for each storm. We carried out TIMEGCM simulations for all four storms and found that the results are similar and consistent with observations. Here we show the results from one storm (17 April 2002) to elucidate the physical mechanisms that cause the storm time MLT temperature changes in middle and low latitudes.

The top panels in Figure 1 give the real Dst (blue line) and Kp values (black line) and a constant Kp value of 3.0 for geomagnetically nondisturbed conditions (red line) between 17 April 2002 and 23 April 2002. The minimum of Dst was −149 nT. The gray areas represent the main phases of the storm (e.g., Balan et al., 2014, 2017). The recovery periods began at 08:00 UT on 18 April and 09:00 UT on 20 April. When the storm occurred at 09:00 UT, the 105°W longitude was at night (02:00 LT, left column), while the 30°E longitude was in the daytime (11:00 LT, right column). For 105°W, T_n at 60°N began to decrease at 10:00 UT and the peak value of T_n decrease was larger than 10 K above 100 km on 17 April. This particular location has a magnetic latitude of 69°N, which was most likely inside the polar cap. This T_n decrease lasted for about 11 hr. T_n then increased at all heights for most of the time from 20:00 UT on 17 April to the storm recovery phase at 15:00 UT on 22 April, with a period of T_n decrease between ~10:00 and 22:00 UT on 19 April. High-latitude T_n began to change when the main phases of the storm started. T_n at 40°N began to change at 09:20 UT on 17 April and continued until 00:00 UT on 23 April. For most of the time, T_n increased and the maximum value of T_n increase at 105 km was 20 K on day 17 April. Interestingly, there are two periods on 17 and 19 April, T_n decreased in some height range. Small T_n decreases are also seen on 22 April. At low latitudes (20°N), T_n increased from 11:00 UT on 17 April to about 00:00 UT on 22 April. T_n changes had about 2-hr time delay compared with the storm onset time. A T_n decrease occurred at higher altitudes on 22 April. The temperature enhancements above ~105 km in the middle and low latitudes were both larger than 10 K. The temporal variations of T_n in middle and low latitudes are similar, while differences do exist. For example, the cooling on 17 and 19 April in middle and high latitudes was absent at low latitudes.

T_n at (60°N, 30°E) began to increase at 15:00 UT (17:00 LT) on 17 April. Unlike the case at 105°W, T_n decrease, with respect to the quiet-time T_n, was small and short lived at this longitude. T_n variations were larger than 5 K above 100 km from 17 to 20 April. T_n changes at middle (40°N) and low latitudes (20°N) were also delayed by about 1 and 2 hr compared with those at high-latitude (60°N). T_n enhancements were larger than 20 K at 40°N and 15 K at 20°N above 105 km during the period of 17–20 April. At both longitudes, T_n increases at middle latitudes were in general larger than those at low latitudes. The time delay of temperature changes increases with decreasing latitudes.

In the left column of Figure 1, the storm began at local night, whereas in the right column, the storm commenced in the local daytime. T_n changes at night occurred earlier than those in the daytime after storm onset. When the storm started at 9:00 UT, the nighttime T_n at 40°N had an immediate response in ~20 min. Whereas, the daytime temperature changes at 40°N occurred at 11:00 LT, which represented a delay of 6 hr from the storm onset. T_n at 30°E began to increase when the region was close to dusk. Thus, the time of temperature response varies with local time.

In the top panel of Figure 2a, T_n enhancements increased with altitude, about 5 K at 105 km and 20 K at 110 km. Moreover, the storm-induced T_n depletion penetrated down to lower altitudes: A T_n change of −5 K can be seen at 94 km between 15:00 and 17:00 UT. Obvious changes in vertical winds occurred at 09:00 UT on 17 April, the storm time winds were more downward at that time. As the differential vertical winds turned from negative/downward to positive/upward at about 11:30 UT, T_n difference reached its maximum values, it then became smaller and negative at 13:30 UT, and attained a minimum value at 16:00 UT, when the differential vertical winds turned from upward to downward. The vertical wind variations occurred down to altitudes as low as 94 km. When the vertical winds became more downward (the differential vertical winds [storm quiet] were negative), T_n differences increased. When they were positive, T_n differences began to decrease. This pattern continued throughout the entire storm period (top two
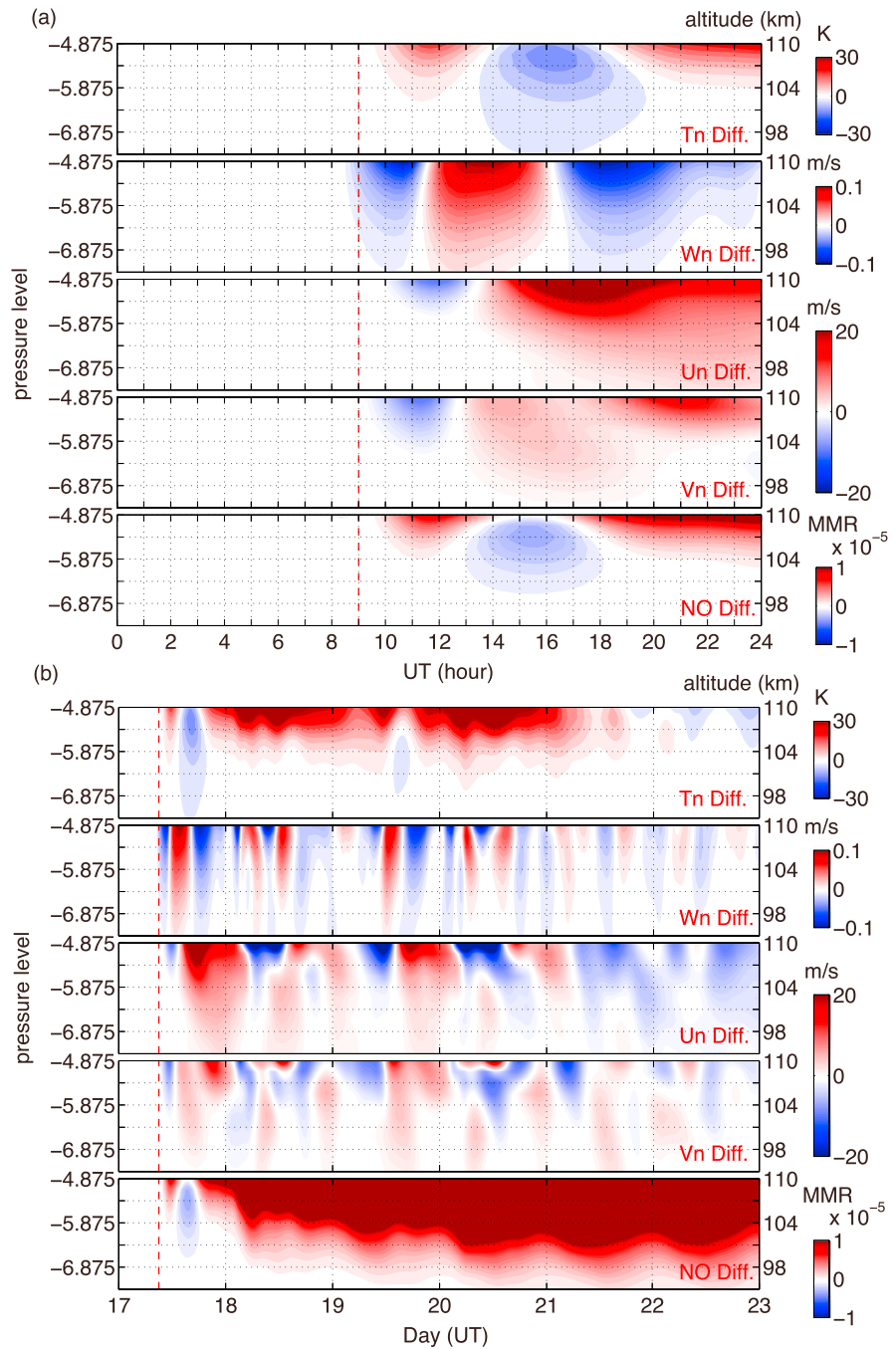
Figure 2. (from top to bottom) Differences of temperature, vertical winds, zonal winds, meridional winds, and NO mass mixing ratio from (a) 0:00 UT to 24:00 UT on 17 April and (b) 17 to 23 April 2002 from 94 to 110 km at the location of (40°N, 105°W).

panels in Figure 2b). This indicates that storm time changes in vertical winds have a strong influence on the behavior of MLT temperatures.

The third panel in Figure 2a shows that large variations of zonal winds occurred at 10:00 UT. Obvious meridional wind changes can also be seen at 09:20 UT (fourth panel). The changes in zonal winds were larger than those of meridional winds. The changes in T_n, horizontal winds, and the peaks of these changes, appear to be later than those of vertical winds after the storm onset from 09:00 UT to 12:00 UT. Note that the occurrence time of zonal wind differences was similar to that of the T_n changes.
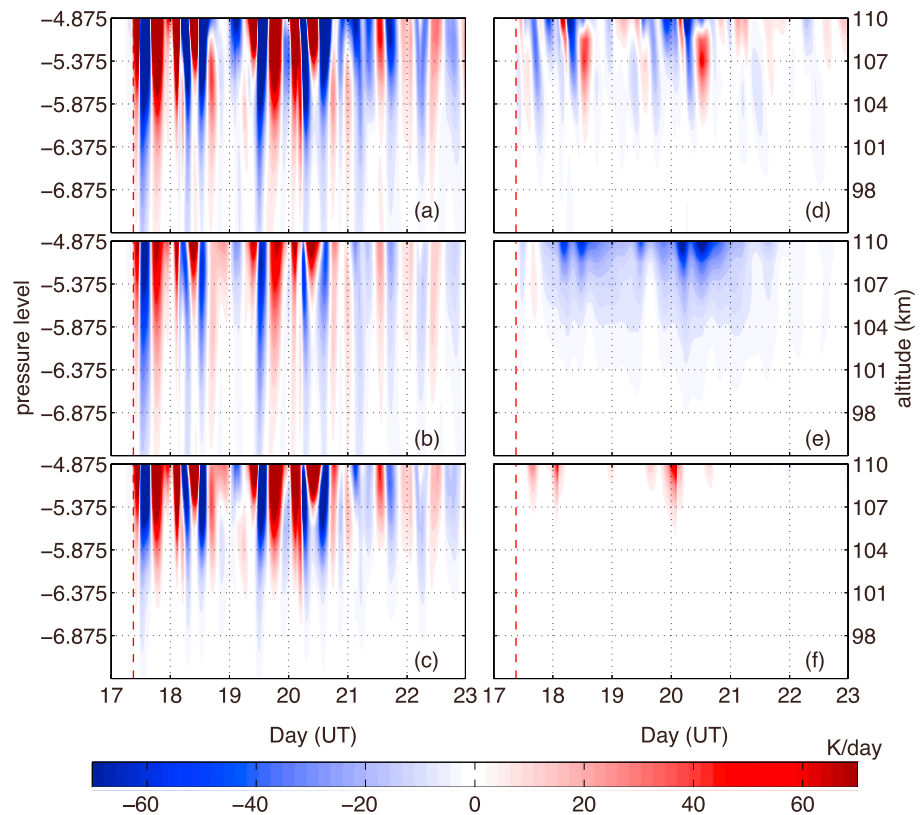
Figure 3. Differences of heating terms: (a) total heating, (b) adiabatic heating/cooling, (c) vertical heat advection, (d) horizontal heat advection, (e) radiative cooling, and (f) Joule heating at the location of (40°N, 105°W).

Radiative cooling in the MLT region is related to NO and CO_2 mass mixing ratio (mmr). The correlation between NO mmr and radiative cooling is much higher than that between CO_2 mmr and radiative cooling. Thus, we just show NO mmr (bottom panels) in Figure 2. NO mmr began to increase at 09:40 UT on 17 April when T_n changed. For most of the time, NO mmr increased, except on 17 April, when NO mmr decreased between 100 and 110 km. The time of decrease coincided with that of T_n decrease. NO mmr increase was small until 02:00 UT of 18 April. This increase lasted until 00:00 UT on 23 April. When the temperature recovered at about 18:00 UT on 21 April, NO mmr still remained enhanced due to its long lifetime (Richards, 2004). It appears that there is not obvious correlation between the trend of NO mmr changes and those of T_n and wind variations after 18 April.

4. Discussion

To understand the mechanisms that cause the storm time MLT temperature changes at middle latitudes, we plot the terms in equation (1) near the lidar station (40°N, 105°W) in Figure 3. The total heating rate (Figure 3a) is the sum of all heating and cooling terms. Figure 3 also shows the differences of five most important terms at the location. The rest of the terms (not shown) contribute negligibly to the overall energy budget.

Figure 3 shows that adiabatic heating/cooling and vertical heat advection are the dominant heating terms. The variations of these two terms were similar, and they responded to the storm almost immediately at the storm onset. Note that the two major heating terms, which are related to vertical winds, changed first in the region, when the storm began (cf. Figure 2a). When the wind circulation at high altitude is modulated by a storm, the change in the circulation expands toward lower latitudes, producing divergent and convergent flow at lower latitudes. The corresponding variations in vertical winds can be either upward or downward. If the vertical wind is downward, adiabatic heating occurs and vertical heat advection increases
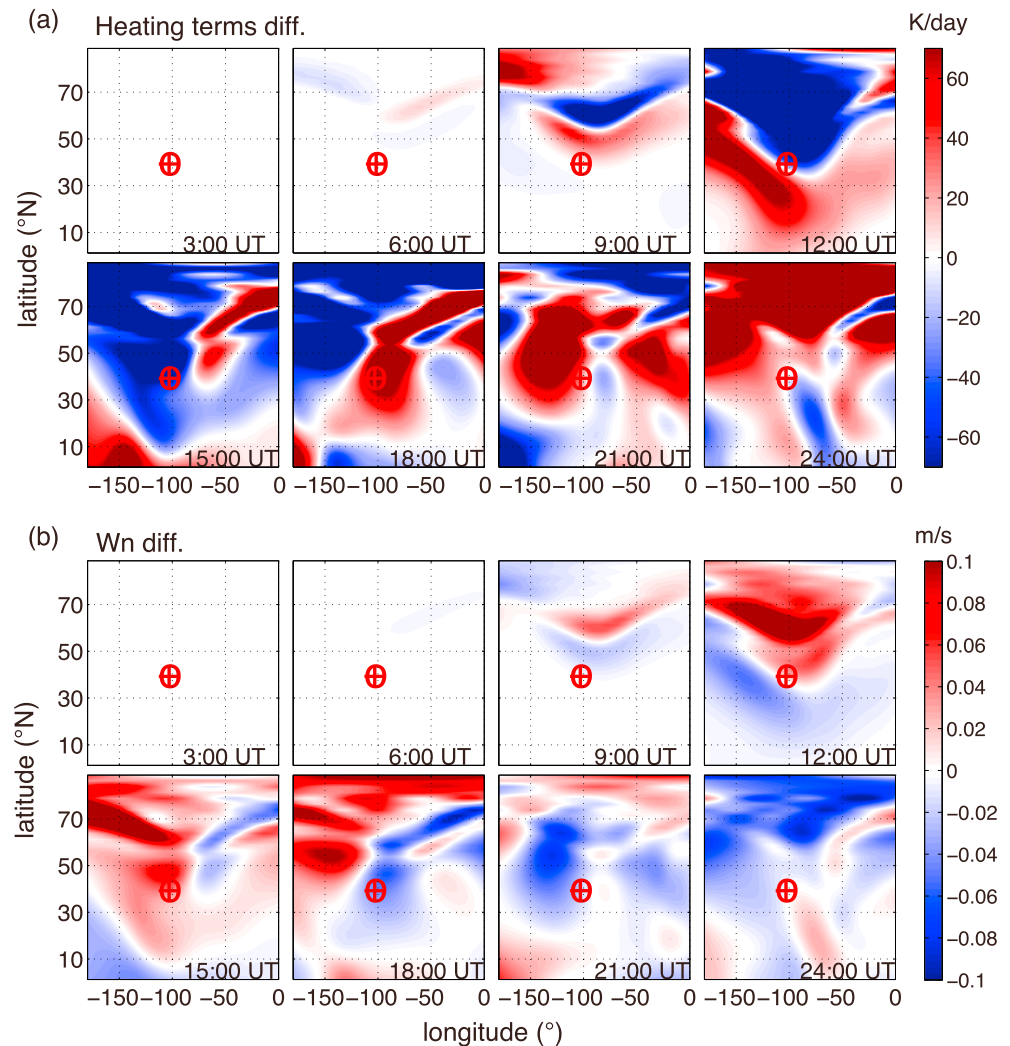
Figure 4. Differences of (a) adiabatic heating/cooling + vertical heat advection and (b) vertical winds at 105 km from 3:00 UT to 24:00 UT on 17 April 2002 in 3-hr intervals. The red crosses give the location of (40°N, 105°W).

when the temperature gradient increases with altitude. Consequently, the storm time total heating increases and temperature is enhanced. In contrast, when the vertical winds are upward, temperature decreases due to adiabatic cooling and vertical heat advection decreases.

Figure 4 illustrates the distributions of the sum of the two major heating terms (adiabatic heating/cooling and vertical heat advection, Figure 4a) and vertical winds (Figure 4b) from 03:00 to 24:00 UT on the storm day of 17 April at 105 km. The red cross indicates the location of the lidar station (40°N, 105°W). When the differential vertical winds were negative or downward (~0.03 m/s at 105 km) at 11:00 UT on 17 April, the effects of the two major heating terms were positive (~60 K/day at 105 km) at the location, which led to a temperature change of about 5 K from 09:00 to 12:00 UT at the beginning of the storm. Three hours later at 15:00 UT, the differential vertical winds changed from negative/downward to positive/upward. The effects of the two major heating terms were cooling (negative). Therefore, adiabatic heating/cooling and vertical heat advection are the results of vertical wind changes and the main causes of T_n variations.

Horizontal heat advection (Figure 3d) is associated with horizontal winds, and the horizontal gradient of T_n. It was relatively small and changed later than the two major heating terms. It is opposite to the temperature changes associated with vertical winds, transports heat into/out of low/high temperature regions, and contributes to the total changes of heating during the storm. When T_n changes, local horizontal winds begin

to converge/diverge due to the changes of horizontal pressure gradient. Thus, variations of horizontal heat advection related to horizontal winds tend to reduce temperature changes.

Radiative cooling acts to lower the temperature. It depends on both NO and CO_2 mmr and temperature changes. However, storm time changes in radiative cooling are mostly associated with NO variations, as CO_2 does not change greatly during storms. The significant variations in radiative cooling, which are caused by temperature variations and the enhancement in NO mmr during the storm, appeared at 19:00 UT on 17 April, much later than the changes in other heating terms. NO cooling becomes large when large changes in temperature occur and NO cooling acts as a thermostat or a refrigerator to prevent temperature from further enhancements. Note that, when temperature increase vanished near 21:00 UT on 21 April, the change of radiative cooling almost disappeared (Figure 3e) at the same time although NO mmr was still enhanced (Figure 2b).

When storms occur, a large amount of solar wind energy is injected into the upper atmosphere at high latitudes. The storm time enhanced ion-neutral collisions and particle precipitation lead to significant Joule heating and particle heating and raise the upper atmospheric temperature in the vicinity of the auroral oval. However, since the lidar station (40°N, 105°W) is subauroral for this storm, Joule heating and particle heating should not have a strong direct impact on temperature at the location. On the other hand, during periods of very strong magnetic activity, the auroral oval can be greatly expanded and this location can become inside the oval, as can be seen in Figure 3f. Joule heating occurred at this location at 18:00 and 24:00 UT on 17 April, and 03:00 UT on 20 April, when Kp was above 7. An enhancement in the Joule heating rate of ~10 K/day occurred near 107 km during those periods. However, compared with other heating terms, Joule heating at this location in the MLT region was relatively weak, its major effects should occur at higher altitudes and latitudes. Therefore, Joule heating cannot be the major direct source for the storm time temperature changes seen in the lower latitudes in the MLT region. This result is consistent with previous studies (e.g., Sinnhuber et al., 2012).

Equatorward of the auroral oval, Joule heating and particle heating are not present to heat the atmosphere directly. Thus, there is a fundamental question that needs to be addressed: What are the physical processes that lead to the observed storm time MLT temperature changes at low and middle latitudes (e.g., Liu et al., 2018; Yuan et al., 2015)? The storm-enhanced electric fields drive a strong ion motion at high latitudes. The large differential motion between the ions and neutrals cause enhanced Joule heating and ion drag, which then drive large changes in T_n and winds in the upper thermosphere (e.g., Huang et al., 2012; Jee et al., 2008). Large latitudinal pressure gradient caused by T_n increases drives a large equatorward meridional circulation at higher altitudes (e.g., Johnson et al., 1987; Kunitake & Schlegel, 1991; Nozawa & Brekke, 1995; Rees, 1972). The enhanced nighttime meridional winds inside the polar cap experience less resistance or ion drag outside the auroral region due to low electron densities, and thus, wind changes can be easily transmitted to lower latitudes at night (Burns et al., 1991; Richmond et al., 2003; Tsuda et al., 2009; Zhang & Shepherd, 2000). During the daytime, T_n is high at lower latitudes due to solar heating, the pressure gradient forcing between high and middle latitudes is in the opposite direction to that generated by high-latitude Joule heating and thus tends to balance out, leading to relatively smaller storm time wind changes. It is thus difficult to transfer heat from high latitudes to lower latitudes by winds in the daytime, and temperatures do not change much until after about local dusk (Burns et al., 1995). Thus, storm time temperature variations at lower latitudes depend on local time. Nighttime temperature changes occur faster than those in the daytime. If a storm starts in the local daytime, temperature changes at lower latitudes in the MLT region may not occur until the local time is near dusk. When high-latitude wind circulation is modulated by a storm and the wind disturbance is transmitted toward lower latitudes, vertical winds in the lower latitudes are changed and can be more downward/upward. Heat is then transferred from higher altitudes into the MLT region by the effects of adiabatic heating/cooling and vertical heat advection. This process is evident in Figure 2: Vertical wind variations occurred prior to the temperature variations at the same height.

5. Conclusion

In this paper, TIMEGCM simulations have been used to study the effects of geomagnetic storms on MLT temperatures at middle and low latitudes. By diagnostically analyzing TIMEGCM outputs in the MLT region during

the 17 April 2002 storm event, we have reached the following conclusions: (1) Both temperature increases and decreases can occur during the storms in the MLT region at low and middle latitudes. (2) The storm time MLT temperature variations depend on local time. Nighttime temperature changes occur faster than those in the daytime. When a storm begins in local daytime, temperature changes at middle and low latitudes may not occur until near dusk. (3) The time delay of temperature changes increases with decreasing latitudes. (4) Adiabatic heating/cooling and vertical heat advection, both associated with changes in vertical winds, are the dominant heating processes at middle and low latitudes in the MLT region during storms. (5) Storm time horizontal heat advection and radiative cooling also contribute to MLT temperature changes at middle and low latitudes. (6) There is no direct contribution of Joule heating and particle heating to the storm time temperature changes equatorward of the auroral oval in the MLT region.

References

Balan, N., Ebihara, Y., Skoug, R., Shiokawa, K., Batista, I. S., Tulasi Ram, S., et al. (2017). A scheme for forecasting severe space weather. *Journal of Geophysical Research: Space Physics*, *122*, 2824–2835. https://doi.org/10.1002/2016JA023853

Balan, N., Skoug, R., Tulasi Ram, S., Rajesh, P. K., Shiokawa, K., Otsuka, Y., et al. (2014). CME front and severe space weather. *Journal of Geophysical Research: Space Physics*, *119*, 10,041–10,058. https://doi.org/10.1002/2014JA020151

Banks, P. M. (1977). Observations of joule and particle heating in the auroral zone. *Journal of Atmospheric and Terrestrial Physics*, *39*(2), 179–193. https://doi.org/10.1016/0021-9169(77)90112-X

Biondi, M. A., & Meriwether, J. W. (1985). Measured response of the equatorial thermospheric temperature to geomagnetic activity and solar flux changes. *Geophysical Research Letters*, *12*(5), 267–270. https://doi.org/10.1029/GL012i005p00267

Burns, A. G., Killeen, T. L., & Roble, R. G. (1991). A theoretical study of thermospheric composition perturbations during an impulsive geomagnetic storm. *Journal of Geophysical Research*, *96*(A8), 14,153–14,167. https://doi.org/10.1029/91JA00678

Burns, A. G., Killen, T. L., Deng, W., Carignan, G. R., & Roble, R. G. (1995). Geomagnetic storm effects in the low- to middle-latitude upper thermosphere. *Journal of Geophysical Research*, *100*(A8), 14,673–14,691. https://doi.org/10.1029/94JA03232

Fagundes, P. R., Sahai, Y., Takahashi, H., Gobbi, D., & Bittencourt, J. A. (1996). Thermospheric and mesospheric temperatures during geomagnetic storms at 23°S. *Journal of Atmospheric and Terrestrial Physics*, *58*(16), 1963–1972. https://doi.org/10.1016/0021-9169(96)00001-3

Fang, X., Randall, C. E., Lummerzheim, D., Solomon, S. C., Mills, M. J., Marsh, D. R., et al. (2008). Electron impact ionization: A new parameterization for 100 eV to 1 MeV electrons. *Journal of Geophysical Research*, *113*, A09311. https://doi.org/10.1029/2008JA013384

Fejer, B. G., Blanc, M., & Richmond, A. D. (2017). Post-storm middle and low-latitude ionospheric electric fields effects. *Space Science Reviews*, *104*(A9), 19,859–19,869. https://doi.org/10.1029/1999JA900271

Förster, M., & Jakowski, N. (2000). Geomagnetic storm effects on the topside ionosphere and plasmasphere: A compact tutorial and new results. *Surveys in Geophysics*, *21*(1), 47–87. https://doi.org/10.1023/A:1006775125220

Fuller-Rowell, T. J., Codrescu, M. V., Moffett, R. J., & Quegan, S. (1994). Response of the thermosphere and ionosphere to geomagnetic storms. *Journal of Geophysical Research*, *99*(A3), 3893–3914. https://doi.org/10.1029/93JA02015

Heelis, R. A., Lowell, J. K., & Spiro, R. W. (1982). A model of the high-latitude ionospheric convection pattern. *Journal of Geophysical Research*, *87*(A8), 6339–6345. https://doi.org/10.1029/JA087iA08p06339

Huang, Y. S., Richmond, A. D., Deng, Y., & Roble, R. (2012). Height distribution of Joule heating and its influence on the thermosphere. *Journal of Geophysical Research*, *117*, A08334. https://doi.org/10.1029/2012JA017885

Jee, G., Burns, A. G., Wang, W., Solomon, S. C., Schunk, R. W., Scherliess, L., et al. (2008). Driving the TING model with GAIM electron densities: Ionospheric effects on the thermosphere. *Journal of Geophysical Research*, *113*, A03305. https://doi.org/10.1029/2007JA012580

Johnson, R. M., Wickwar, V. B., Roble, R. G., & Luhmann, J. G. (1987). Lower-thermospheric winds at high latitude: Chatanika radar observations. *Annales de Geophysique*, *5*, 383–404.

Kunitake, M., & Schlegel, K. (1991). Neutral winds in the lower thermosphere at high latitudes from five years of EISCAT data. *Annales de Geophysique*, *9*, 143–155.

Liu, J., Wang, W., Burns, A., Yue, X., Zhang, S., & Huang, C. (2016). Profiles of ionospheric storm-enhanced density furing the 17 March 2015 great profiles of ionospheric storm-enhanced density during the 17 March great storm. *Journal of Geophysical Research: Space Physics*, *121*, 727–744. https://doi.org/10.1002/2015JA021832

Liu, X., Yue, J., Wang, W., Xu, J., Zhang, Y., Li, J., et al. (2018). Responses of lower thermospheric temperature to the 2013 St. Patrick's Day geomagnetic storm. *Geophysical Research Letters*, *45*, 4656–4664. https://doi.org/10.1029/2018GL078039

Mendillo, M., Papagiannis, M. D., & Klobuchar, J. A. (1972). Average behavior of the midlatitude F-region parameters NT, Nmax and τ during geomagnetic storms. *Journal of Geophysical Research*, *77*(25), 4891–4895. https://doi.org/10.1029/JA077i025p04891

Nesse Tyssøy, H., Heinrich, D., Stadsnes, J., Sørbø, M., Hoppe, U.-P., Evans, D. S., et al. (2008). Upper-mesospheric temperatures measured during intense substorms in the declining phase of the January 2005 solar proton events. *Annales de Geophysique*, *26*(9), 2515–2529. https://doi.org/10.5194/angeo-26-2515-2008

Nesse Tyssøy, H., Stadsnes, J., Sørbø, M., Mertens, C. J., & Evans, D. S. (2010). Changes in upper mesospheric and lower thermospheric temperatures caused by energetic particle precipitation. *Journal of Geophysical Research*, *115*, A10323. https://doi.org/10.1029/2010JA015427

Nozawa, S., & Brekke, A. (1995). Studies of the E region neutral wind in the disturbed auroral ionosphere. *Journal of Geophysical Research*, *100*(A8), 14,717–14,734. https://doi.org/10.1029/95JA00676

Pancheva, D., Singer, W., & Mukhtarov, P. (2007). Regional response of the mesosphere-lower thermosphere dynamics over Scandinavia to solar proton events and geomagnetic storms in late October 2003. *Journal of Atmospheric and Terrestrial Physics*, *69*(9), 1075–1094. https://doi.org/10.1016/j.jastp.2007.04.005

Rees, D. (1972). Winds and temperatures in the auroral zone and their relations to geomagnetic activity. *Home | Philosophical Transactions of the Royal Society of London*, *A71*, 563–575.

Rees, M. H., Emery, B. A., Roble, R. G., & Stamnes, K. (1983). Neutral and ion gas heating by auroral electron precipitation. *Journal of Geophysical Research*, *88*(A8), 6289–6300. https://doi.org/10.1029/JA088iA08p06289

Richards, P. G. (2004). On the increase in nitric oxide density at midlatitudes during ionospheric storm. *Journal of Geophysical Research*, *109*, A06304. https://doi.org/10.1029/2003JA010110

Richmond, A. D., Lathuillere, C., & Vennerstroem, S. (2003). Winds in the high-latitude lower thermosphere: Dependence on the interplanetary magnetic field. *Journal of Geophysical Research*, *108*(A2), 1066. https://doi.org/10.1029/2002JA009493

Roble, R. G., Emery, B. A., Killeen, T. L., Reid, G. C., Solomon, S., Garcia, R. R., et al. (1987). Joule heating in the mesosphere and thermosphere during the July 13, 1982, solar proton event. *Journal of Geophysical Research*, *92*(A6), 6083–6090. https://doi.org/10.1029/JA092iA06p06083

Roble, R. G., & Ridley, E. C. (1994). A thermosphere-ionosphere-mesosphere-electrodynamics general circulation model (time-GCM): Equinox solar cycle minimum simulations (30–500 km). *Geophysical Research Letters*, *21*(6), 417–420. https://doi.org/10.1029/93GL03391

Sinnhuber, M., Nieder, H., & Wieters, N. (2012). Energetic particle precipitation and the chemistry of the mesosphere/lower thermosphere. *Surveys in Geophysics*, *33*(6), 1281–1334. https://doi.org/10.1007/s10712-012-9201-3

Tsuda, T. T., Nozawa, S., Oyama, S., Motoba, T., Ogawa, Y., Shinagawa, H., et al. (2009). Acceleration mechanism of high-speed neutral wind observed in the polar lower thermosphere. *Journal of Geophysical Research*, *114*, A04322. https://doi.org/10.1029/2008JA013867

Von Savigny, C., Sinnhuber, M., Bovensmann, H., Burrows, J. P., Kallenrode, M. -B., & Schwartz, M. (2007). On the disappearance of noctilucent clouds during the January 2005 solar proton events. *Geophysical Research Letters*, *34*, L02805. https://doi.org/10.1029/2006GL028106

Xu, J. Y., Smith, A. K., & Wang, W. (2013). An observational and theoretical study of the longitudinal variation in neutral temperature induced by aurora heating in the lower thermosphere. *Journal of Geophysical Research: Space Physics*, *118*, 7410–7425. https://doi.org/10.1002/2013JA019144

Yuan, T., Zhang, Y., Cai, X., She, S. -Y., & Paxton, L. J. (2015). Impacts of CME-induced geomagnetic storms on the midlatitude mesosphere and lower thermosphere observed by a sodium lidar and TIMED/GUVI. *Geophysical Research Letters*, *42*, 7295–7302. https://doi.org/10.1002/2015GL064860

Zhang, S. P., & Shepherd, G. G. (2000). Neutral winds in the lower thermosphere observed by WINDII during the April 4–5th, 1993 storm. *Geophysical Research Letters*, *27*(13), 1855–1858. https://doi.org/10.1029/2000GL000034